Digital Twin-Based Proactive Resource Management for Integrated Sensing and Communication

Shisheng Hu, *Student Member, IEEE*, Jie Gao, *Senior Member, IEEE*, Xue Qin, *Student Member, IEEE*, Conghao Zhou, *Member, IEEE*, Xinyu Huang, *Student Member, IEEE*, Mushu Li, *Member, IEEE*, Mingcheng He, *Student Member, IEEE*, and Xuemin (Sherman) Shen, *Fellow, IEEE*

Abstract—Leveraging the integrated sensing and communication (ISAC) paradigm, wireless networks can provide sensing and communication services, which are essential for industrial cyber-physical systems (CPSs). However, non-stationary distributions of the mobile ISAC devices and sensing targets in industrial environments make the service provision challenging. In this paper, we propose a digital twin (DT)-based resource reservation scheme for ISAC in CPSs, aiming at satisfying service demands with minimal reserved network resources. Particularly, we first design a DT-based spatial distribution modeling approach that adaptively synergizes multiple candidate spatial models to tackle the challenge of non-stationary distributions. We then develop a location-based resource-efficient approach to collaborative sensing, reserving shared spectrum resources for ISAC devices to track sensing targets in their close proximity. Finally, we derive closed-form formulas for efficiently obtaining candidate resource reservation decisions, and propose a DT-based network emulation approach to evaluate the candidate decisions and select the optimal one. Numerical results show that the proposed DT-based resource reservation scheme can increase service satisfaction ratio by up to 18% and reduce resource consumption by up to 11.5% compared with benchmark schemes.

Index Terms—Digital twin, integrated sensing and communication, proactive resource management, industrial cyber-physical systems.

I. INTRODUCTION

Sensing and communication are essential functions that support real-time monitoring and control in industrial cyber-physical systems (CPSs) [2], [3]. Recent advancements in wireless networks, such as the exploitation of large-scale antenna arrays, higher frequency bands, and networked computing, have catalyzed the transformative integrated sensing and communication (ISAC) paradigm [4]. In this paradigm, wireless network infrastructures and end devices can perform both communication and environmental sensing functions. ISAC can enhance resource utilization efficiency in CPSs through resource sharing. In addition, ISAC can improve sensing signal propagation in adverse weather conditions [5],

enhance sensing signal processing through networked computing [6], and increase communication efficiency by leveraging environment knowledge [7].

Providing satisfactory sensing services along with existing communication services by a wireless network requires efficient management and utilization of network resources. The radio access network (RAN) slicing-based resource management framework can be used to isolate and better support the provision of the communication and the sensing services [8]. In addition, ISAC access points (APs) and devices in a wireless network should collaborate efficiently while exploiting their unique strengths in sensing [5]. In particular, ISAC devices, e.g., mobile robots, usually have closer proximity to the targets, e.g., human workers, which results in lower required sensing signal power and a higher potential for spatial reuse of spectrum resources. In contrast, ISAC APs, hereafter referred to as APs, typically have larger antenna arrays and more computing resources for sensing data processing.

Information on the spatial distributions of mobile ISAC devices and targets is crucial for resource management for ISAC in a CPS. First, the spatial distributions of ISAC devices and targets reflect the sensing and communication service demands. Second, the distances between the targets and the ISAC devices, as well as that between the targets and the APs, determine the association of targets with them. Third, the spatial distribution of ISAC devices determines the interference level if they reuse the same spectrum band for sensing [9], [10]. A statistical model to characterize the spatial distributions, referred to as a spatial model, is necessary for proactive resource management, i.e., large-timescale resource reservation in RAN slicing [11]. Obtaining such a spatial model, referred to as spatial modeling, is challenging due to the potentially non-stationary spatial distributions in industrial environments [12]. For example, the safe separation distances between robots and human workers may change dynamically based on factors such as human and robot velocities [13] and specific task requirements [14].

Most works on spatial modeling-based resource management for ISAC, e.g., [9], [15]–[20], rely on a temporally stationary spatial model with constant and known model parameters. Nevertheless, in the presence of the temporal non-stationarity, relying on a single spatial model is susceptible to *model drift*, i.e., degradation of model accuracy due to changes in data distribution over time [21], and potentially compromises the effectiveness of resource reservation decisions. As a result, adaptive spatial modeling and accurate evaluation of

Shisheng Hu, Xue Qin, Conghao Zhou, Xinyu Huang, Mingcheng He, and Xuemin (Sherman) Shen are with the Department of Electrical and Computer Engineering, University of Waterloo, Waterloo, ON N2L 3G1, Canada (email: {s97hu, x7qin, c89zhou, x357huan, m64he, sshen}@uwaterloo.ca).

Jie Gao is with the School of Information Technology, Carleton University, Ottawa, ON K1S 5B6, Canada (email: jie.gao6@carleton.ca).

Mushu Li is with the Department of Computer Science and Engineering, Lehigh University, Bethlehem, PA 18015, USA (email: mul224@lehigh.edu).

Part of this research work was presented at the IEEE/CIC International Conference on Communications in China (ICCC), 2024 [1].

(Corresponding author: Conghao Zhou.)

resource reservation decisions derived based on the modeling are necessary. To achieve this goal, the digital twin (DT) paradigm, an emerging paradigm for network virtualization and management [22], can be exploited. In particular, DTs of network slices can be established as digital representations of the network slices to collect and process the data from the corresponding slices, e.g., data pertaining to the service demand, and generate slice-level management decisions [23], [24]. In addition, based on the collected data, simulation environments can be established for evaluating resource management decisions [25], [26].

In this paper, we propose a novel DT-based resource reservation scheme for ISAC in an industrial CPS. Our objective is to reserve the minimum spectrum and edge computing resources for the network slices of sensing and communication while satisfying the service demands in the CPS. To achieve this objective, we establish DTs of the network slices, where spatial modeling and network slice instances are obtained by collecting and processing the location data of ISAC devices and targets. In the spatial modeling, we exploit multiple point process-based spatial models to tackle the model drift in predicting the parameters in individual spatial models. Leveraging the network slice instances, we propose a network emulation approach to evaluate candidate resource reservation decisions given different spatial models and select the optimal one. Numerical results demonstrate that the proposed scheme can enhance service demand satisfaction and reduce resource consumption compared with benchmark schemes. The contributions of this paper are summarized as follows.

1) We design a DT-based spatial modeling approach for industrial CPSs that monitors the drift in multiple point process-based spatial models, and tackles the model drift by the update and ensemble of the spatial models.

2) Leveraging the spatial modeling, we develop a resource-efficient approach to device-AP collaborative sensing, where ISAC devices reuse spectrum resources to track targets in their close proximity. In addition, closed-form formulas for efficiently generating candidate resource reservation decisions are derived.

3) The proposed DT-based network emulation enables the synergy of multiple spatial models for resource reservation, by efficiently and accurately evaluating and selecting from the candidate resource reservation decisions given each of the spatial models.

The remainder of this paper is organized as follows. In Section II, we review the related works. In Section III, we present the system model and formulate the resource reservation problem. The DTs of network slices for adaptive spatial modeling are introduced in Section IV. The resource reservation scheme based on the slice DTs is detailed in Section V. Simulation results are provided in Section VI, followed by the conclusion of this paper in Section VII.

II. RELATED WORKS

A. Resource Management for ISAC

To implement the ISAC paradigm, there are primarily two kinds of approaches: unified waveform design and non-overlapping resource allocation [27], [28]. In the unified waveform design approach, the sensing and communication functions are implemented via a single signal waveform. This approach may achieve a high spectrum and energy efficiency, but introduces high complexity for real-time waveform optimization [27]. In the non-overlapping resource allocation approach, spectrum resources are individually allocated, in the time, frequency, and beam domains, to transmit sensing and communication signals. Although the resource utilization efficiency may be lower, this approach is simpler to implement and thus receive considerable attention [27]–[32].

To capture service demands and effectively manage resources for ISAC, information on the spatial distributions of sensing nodes and targets is crucial [28]. In particular, prior information on the real-time locations of sensing nodes and targets facilitate real-time resource management, e.g., beam management [33], power control [31]–[33], and spectrum allocation [31], [32]. For proactive resource management, i.e., resource reservation [11], [23], it is crucial to employ spatial modeling of sensing nodes and targets to capture the randomness of their locations during a reservation window. Point processes that are temporally stationary, i.e., those with constant parameters over time, are commonly used [34]. Then, the formulas for estimating spatially averaged sensing and communication performances, e.g., target detection probability and ergodic transmission rate, can be derived, accordingly [9], [19], [20]. The performance estimation formulas are then utilized to make resource reservation decisions, e.g., time allocation in time-division-based ISAC systems [15], the density of APs [16], [17], and the clustering of APs for interference management in multi-cell dense wireless networks [18].

Different from the existing works, we investigate the spatial modeling in temporally non-stationary environments within industrial CPSs. We develop adaptive update and synergy of multiple temporally non-stationary point processes in the spatial modeling and resource reservation for ISAC.

B. DT-Assisted Resource Management

The DT paradigm was recently proposed to support resource management in wireless networks [22]. A DT involves a digital representation of a physical object and the synchronization between them. Existing works establish DTs of users and network slices to capture their real-time or statistical characteristics, e.g., user swiping behaviour in short video streaming [24], user mobility pattern in mobile edge computing applications [23], sensing devices' data quality in collaborative sensing [35], user-AP link quality in heterogenous networks [36], and end-to-end delay in network slices [37]. In addition, DTs are used for network emulation to augment the training data of data-driven resource management schemes in [26]. Another important research issue is addressing the challenges in establishing DTs. To obtain sufficient data about users, user location data is collected in [38], and generative Artificial Intelligence is used for generating user trajectory data [25]. To enhance resource efficiency, the selection of data attributes and data processing methods for the establishment of DTs are investigated in [36] and [39], respectively.
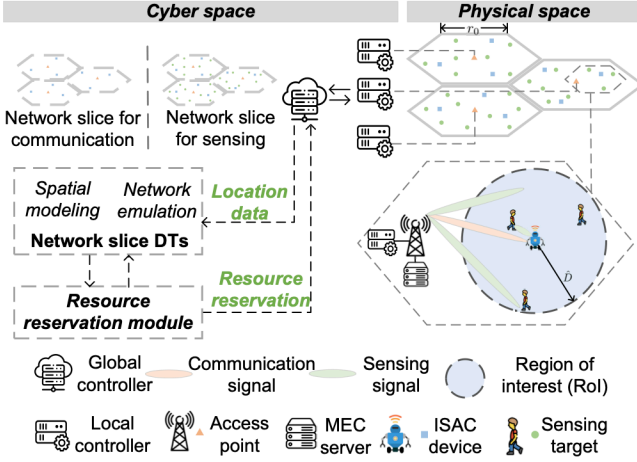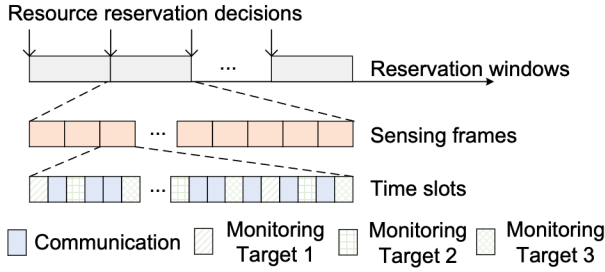
Fig. 1: Architecture of the industrial CPS.

Fig. 2: An illustrative example of timescales, where an ISAC device is associated with three targets at the beginning of the sensing frame.

Different from the existing works, to cope with the temporal non-stationarity, we explore how DTs of network slices can be adaptively configured to output an appropriate spatial model to reserve resources for ISAC in industrial CPSs. In addition, we investigate how the DTs can be used in network emulation to evaluate candidate resource reservation decisions.

III. SYSTEM MODEL AND PROBLEM FORMULATION

A. System Architecture

We consider an industrial CPS, which is illustrated in Fig. 1. In the physical space of the industrial CPS, we consider an industrial zone where a cluster of L APs is deployed. The APs cover non-overlapping areas to provide sensing and communication services. Each area is a hexagon with a side length r_0 and an area of $A_0 = 3\sqrt{3}r_0^2/2$. Each AP coordinates a mobile edge computing (MEC) server. In addition, in the coverage of each AP, there are mobile robots as ISAC devices with sensing, communication, and computing capabilities, and human workers as targets. To enhance workspace safety and efficiency, sensing services are required for the targets in the RoI, as a circle with radius $\hat{D}$, of each ISAC device. Each AP searches for the targets that newly arrive within the RoIs in its coverage. In addition, to improve resource utilization efficiency, each AP collaborates with the ISAC devices in its coverage, that adopt a time-division ISAC scheme [29], [30], to track the state of the targets including the location, velocity, and activity.

In the cyber space of the industrial CPS, distributed local controllers at each AP and a centralized global controller at the remote cloud aggregate and process data from the physical space, and generate control decisions to be implemented. We specifically focus on the controllers' role in managing the spectrum and edge computing resources in wireless networks for providing sensing and communication services. To efficiently guarantee their respective quality of service, RAN slicing-based resource management framework is adopted. Particularly, two network slices are established to provide sensing and communication services, respectively. The management of the network slices involves making decisions across three different timescales by the controllers. As shown in Fig. 2, the timescales include reservation windows (indexed by $k \in \{1, 2, 3, ..., K\}$), sensing frames (indexed by $m \in \{1, 2, 3, ..., M\}$), and time slots, arranged in descending order of their durations. Specifically, each reservation window consists of M frames; each frame consists of T slots; and each slot is τ seconds in length. The three types of network management decisions corresponding to the three timescales are summarized as follows.

- At the beginning of each reservation window, the global controller reserves spectrum and edge computing resources for the slices, respectively.
- At the beginning of each sensing frame, for updating the status of each individual target in the RoI of each ISAC device, the local controller at the corresponding AP associates the target with either the AP or the ISAC device.
- At the beginning of each time slot, each ISAC device in the coverage of an AP is scheduled by the local controller at the AP to perform either sensing or communication throughout the time slot.

In this paper, we focus on proactive resource management for ISAC in the industrial CPS, i.e., the resource reservation made by the global controller for the sensing and communication slices at the beginning of each reservation window. To make such decisions, the spatial distributions of ISAC devices and targets, that are dynamic in each reservation window due to their mobility, need to be characterized. As shown in Fig. 1, the global controller aggregates the location data of ISAC devices and targets in each network slice to establish DTs of the network slices. The DTs are used to achieve adaptive spatial modeling and network emulation, to be detailed in Section IV. A resource reservation module in the global controller leverages the DTs for making the resource reservation decision, to be detailed in Section V.

B. Communication Model

The global controller reserves $X_c^A \in \mathbb{Z}_{\geq 0}$ subcarriers for the uplink communication of the ISAC devices in the coverage of each AP. The total amount of spectrum resources reserved for the uplink communication in the coverage of the L APs is thus $Z_c^A = L \cdot X_c^A \cdot B_{c,0}$, where $B_{c,0}$ is the bandwidth of each subcarrier in Hertz. We consider the scenario where there exists at least one ISAC device in the coverage of each AP. Consider the homogeneity among different ISAC devices and APs, respectively. We focus on one representative ISAC device and one representative AP when deriving the service demands and capacities, and refer to them as the ISAC device and the AP, respectively. The number of ISAC devices in the coverage

of the AP is denoted by N^{I}. At the beginning of each time slot, with an active probability $\rho_{\mathrm{c}} \in (0,1]$, each ISAC device in the coverage of each AP is scheduled by the local controller at the AP for uplink communication. The number of all ISAC devices that are scheduled for communication in the time slot is denoted by $N_{\mathrm{c}}^{\mathrm{I}}$. Conditioning on that $N^{\mathrm{I}} = n$ and the ISAC device is scheduled for uplink communication, the probability mass function (PMF) of $N_{\mathrm{c}}^{\mathrm{I}}$ is

$$\mathbb{P}\{N_{\mathrm{c}}^{\mathrm{I}} = n_{\mathrm{c}} | N^{\mathrm{I}} = n\} = \binom{n_{\mathrm{c}} - 1}{n - 1} \rho_{\mathrm{c}}^{n_{\mathrm{c}} - 1} (1 - \rho_{\mathrm{c}})^{n - n_{\mathrm{c}}}, \quad (1)$$

where $n_{\mathrm{c}} = 1, 2, 3, ..., n$, and $n = 1, 2, ...$. As a result, we have $\mathbb{E}\left[N_{\mathrm{c}}^{\mathrm{I}} \middle| N^{\mathrm{I}}\right] = 1 + (N^{\mathrm{I}} - 1)\rho_{\mathrm{c}}$. The subcarriers are evenly allocated to the ISAC devices scheduled for communication, and the number of the subcarriers allocated to the ISAC device is $X_{\mathrm{c}}^{\mathrm{I}} = X_{\mathrm{c}}^{\mathrm{A}}/N_{\mathrm{c}}^{\mathrm{I}}$.

Proposition 1: *Denote the transmission rate over each subcarrier (in bits per time slot) by R_0 and the uplink transmission of the ISAC device by R. A lower bound of the expectation of transmission rate R is*

$$\bar{R} = \rho_{\mathrm{c}} \cdot \frac{R_0 X_{\mathrm{c}}^{\mathrm{A}}}{1 + (\mathbb{E}[N^{\mathrm{I}}] - 1)\rho_{\mathrm{c}}}. \quad (2)$$

Proof: Please refer to Appendix A. ∎

The lower bound in (2), i.e., $\bar{R}$, corresponds to the communication service capacity. The average amount of data that each ISAC device needs to upload per time slot, denoted by $\hat{R}$, corresponds to the communication service demand.

C. Sensing Model

We consider two kinds of sensing tasks. The first kind is the *target searching task*. Particularly, in each sensing frame, the AP searches for the targets that newly arrive at the RoIs of the ISAC devices in its coverage. At the end of each sensing frame, based on the search results, the local controller at the AP updates a database that catalogs the targets within the RoIs of the ISAC devices in its coverage. The second kind is the *target tracking task*. In particular, within a sensing frame, a target from the database is associated with either an ISAC device or the AP for monitoring across multiple time slots. At the end of each of the time slots, a sensing data sample is collected for the target. At the end of the frame, the accumulated sensing data samples for each target are processed to determine the state of the target. The tracking results are recorded in the target database, providing prior information to facilitate target tracking in subsequent sensing frames.

1) Target Searching and Tracking by APs: The AP performs digital beamforming to simultaneously form multiple beams. To avoid the inter-beam interference, different beams are allocated with orthogonal sensing spectrum bands [31], [32], each having the bandwidth $B_{\mathrm{s},0}$. For the AP, a constant number of $\widehat{X}_{\mathrm{s}}^{\mathrm{A}}$ spectrum bands are reserved to form $\widehat{X}_{\mathrm{s}}^{\mathrm{A}}$ search beams to search for targets that newly arrive at the RoIs of ISAC devices in each sensing frame [40]. In addition, $X_{\mathrm{s}}^{\mathrm{A}}$ spectrum bands are reserved for each AP to form $X_{\mathrm{s}}^{\mathrm{A}} \in \mathbb{Z}_{\geq 0}$ track beams, each of which can be used to track one associated target [31], [40]. The total amount of spectrum resources

reserved for target searching and tracking by the L APs, denoted by $Z_{\mathrm{s}}^{\mathrm{A}}$, is $Z_{\mathrm{s}}^{\mathrm{A}} = L \cdot (\widehat{X}_{\mathrm{s}}^{\mathrm{A}} + X_{\mathrm{s}}^{\mathrm{A}}) \cdot B_{\mathrm{s},0}$.

2) Target Tracking by ISAC Devices: For tracking the targets by the ISAC devices in the coverage of the L APs, the global controller reserves $X_{\mathrm{s}}^{\mathrm{I}} \in \mathbb{Z}_{\geq 0}$ spectrum bands, each having bandwidth $B_{\mathrm{s},0}$. As a result, the total amount of spectrum resources reserved for target tracking by all the ISAC devices is $Z_{\mathrm{s}}^{\mathrm{I}} = X_{\mathrm{s}}^{\mathrm{I}} \cdot B_{\mathrm{s},0}$. At the beginning of a time slot, an ISAC device will enter the sensing mode if not scheduled by the local controller for communication, the probability of which is $1 - \rho_{\mathrm{c}}$. Similar to [10], in each time slot, the ISAC device in the sensing mode randomly chooses one of the $X_{\mathrm{s}}^{\mathrm{I}}$ reserved spectrum bands with equal probability $1/X_{\mathrm{s}}^{\mathrm{I}}$, and forms a track beam towards one associated target [30].

We consider the following beam pattern of ISAC devices in the sensing mode. The width of the beam is ϕ_{I}, and the antenna gain is $G_{\mathrm{m}} = G_0 2\pi/\phi_{\mathrm{I}}$ in the beam, and zero elsewhere [41]. The power of the signal reflected from a target received at the ISAC device, denoted by P_{e}, can be calculated by $P_{\mathrm{e}} = P_{\mathrm{s}} G_{\mathrm{m}}^2 c^2 \bar{\sigma}/(4\pi)^3 f_{\mathrm{s}}^2 D^4$ [9], where P_{s} represents the transmit power of sensing signals; c represents the speed of light; $\bar{\sigma}$ represents the average value of radar cross section (RCS) of the target; f_{s} represents the centre frequency of the accessed spectrum band; D represents the distance between the ISAC device and the target. The ISAC device in the sensing mode will receive the interference from any other ISAC device that is also in the sensing mode, accessing the same spectrum band for sensing, and residing within each other's beams. For tractability, we consider only the strongest interfering signal to the ISAC device, which is the signal from the nearest ISAC device. The power of the interference signal is denoted by I_{s}, and the signal-to-interference ratio (SIR) is denoted by γ_{s} and calculated as $\gamma_{\mathrm{s}} = P_{\mathrm{e}}/I_{\mathrm{s}}$.

3) Sensing Data Processing: At the end of each sensing frame, the accumulated sensing data samples for each target need to be processed by methods including parameter estimation [27] and pattern recognition [26] to extract the motion state of the target. The total computational overhead for processing the sensing data of one target is denoted by C_0 in CPU cycles. The constant computational capability of each ISAC device in CPU cycles per second is denoted by $F_{\mathrm{e}}^{\mathrm{I}}$. For processing the sensing data collected by each AP, the amount of reserved edge computing resources at the AP is denoted by $F_{\mathrm{e}}^{\mathrm{A}}$. The total amount of edge computing resources reserved for the L APs is $Z_{\mathrm{e}}^{\mathrm{A}} = L \cdot F_{\mathrm{e}}^{\mathrm{A}}$. The delay in processing the sensing data collected by the ISAC device and the AP within a sensing frame, denoted by $T_{\mathrm{e}}^{\mathrm{I}}$ and $T_{\mathrm{e}}^{\mathrm{A}}$, respectively, is calculated as $T_{\mathrm{e}}^{\mathrm{I}} = N_{\mathrm{I}}^{\mathrm{U}} C_0/F_{\mathrm{e}}^{\mathrm{I}}$, and $T_{\mathrm{e}}^{\mathrm{A}} = N_{\mathrm{A}}^{\mathrm{U}} C_0/F_{\mathrm{e}}^{\mathrm{A}}$. Here, $N_{\mathrm{A}}^{\mathrm{U}}$ and $N_{\mathrm{I}}^{\mathrm{U}}$ represent the numbers of targets that are associated with the AP and the ISAC device at the beginning of a sensing frame.

4) Sensing Requirements: Multi-dimensional requirements, including the quality, quantity, and processing delay of sensing data, are considered for the sensing service.

First, to successfully extract the information of a target from the sensing data samples, the SIR should be greater than a threshold $\widehat{\gamma}_{\mathrm{s}}$. Consider the randomness in the SIR across dif-
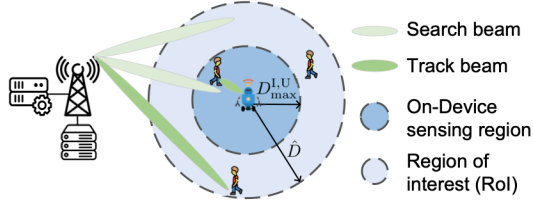
Fig. 3: Sensing model and sensing region division.

ferent sensing data samples, we adopt the following constraint on the quality of sensing data [20]: $\mathbb{P}\{\gamma_s \geq \widehat{\gamma}_s\} \geq \widehat{P}$.

Second, to obtain sufficient sensing data samples about each target, the number of time slots assigned to track the target in a sensing frame must exceed a threshold. We denote the threshold on the average number of times each target is tracked per time slot by $\widehat{\rho}_s \in (0, 1]$ [29]. In each time slot, the expected number of track attempts that are conducted by the ISAC device is $1 - \rho_c$ times, and that by the AP is X_s^A times. As a result, the expected numbers of targets associated with the ISAC device and that associated with the AP should respectively satisfy the two following constraints:

$$\mathbb{E}\left[N_I^U\right] \leq \frac{1 - \rho_c}{\widehat{\rho}_s}; \quad \mathbb{E}\left[N_A^U\right] \leq \frac{X_s^A}{\widehat{\rho}_s}. \quad (3)$$

Third, to guarantee the freshness of sensing results, the expected sensing data processing delay at the ISAC device and the AP, i.e., $\mathbb{E}\left[T_e^I\right]$ and $\mathbb{E}\left[T_e^A\right]$, should be less than the duration of a sensing frame, or equivalently, T time slots:

$$\frac{\mathbb{E}\left[N_I^U\right] C_0}{F_e^I} \leq \tau T; \quad \frac{\mathbb{E}\left[N_A^U\right] C_0}{F_e^A} \leq \tau T. \quad (4)$$

5) Sensing Region Division-Based Target Association: With an increasing distance between an ISAC device and a target, the power of the received sensing signal from the target decreases, which leads to a higher chance of violating the SIR requirement. To this end, as shown in Fig. 3, we draw a concentric inner circle with radius $D_{\max}^{I,U}$ in the RoI of each ISAC device and define it as the *on-device sensing region*. A target will be associated with the ISAC device only if it is *(i)* in the on-device sensing region of the ISAC device and *(ii)* nearest to the ISAC device than to any other ISAC devices. By properly determining the radius of the on-device sensing region, the SIR requirement can be satisfied. With such association, the expected number of targets that can be associated with the ISAC device should satisfy the constraint:

$$\mathbb{E}\left[N_I^U\right] \leq \mathbb{P}\left\{D^{I,U} \leq D_{\max}^{I,U}\right\} \cdot \mathbb{E}\left[N_{I,1}^U\right], \quad (5)$$

where $D^{I,U}$ represents the distance between a target to its closest ISAC device; $\mathbb{P}\{D^{I,U} \leq D_{\max}^{I,U}\}$ is the probability that the distance is smaller than the radius of the on-device sensing region; $\mathbb{E}\left[N_{I,1}^U\right]$ is the expected number of targets that are closer to the ISAC device than to any other ISAC devices.

6) Sensing Service Demand and Capacity: The number of the targets in the RoIs in the coverage of the AP is denoted by N^U. The expectation of N^U corresponds to the sensing service demand in the coverage of the AP. The demand is calculated by multiplying the expected number of ISAC devices with that of the targets within the RoI for each ISAC device:

$$\mathbb{E}\left[N^U\right] = \mathbb{E}\left[N^I\right] \cdot \left(\mathbb{P}\{D^{I,U} \leq \hat{D}\} \cdot \mathbb{E}\left[N_{I,1}^U\right]\right), \quad (6)$$

where $\mathbb{P}\{D^{I,U} \leq \hat{D}\}$ is the probability that the distance between a target to the closest ISAC device is smaller than the radius of the RoI of the ISAC device.

Combining the constraint on sensing quantity in (3), the constraint on sensing data processing delay in (4), and the constraint due to the maximum number of targets in the on-device sensing region in (5), we derive the maximum values of $\mathbb{E}[N_I^U]$ and $\mathbb{E}[N_A^U]$ as

$$\overline{N}_I^U \triangleq \min\left\{\mathbb{P}\left\{D^{I,U} \leq D_{\max}^{I,U}\right\} \cdot \mathbb{E}\left[N_{I,1}^U\right], \frac{1 - \rho_c}{\widehat{\rho}_s}, \frac{\tau T \cdot F_e^I}{C_0}\right\}, \quad (7a)$$

and

$$\overline{N}_A^U \triangleq \min\left\{\frac{X_s^A}{\widehat{\rho}_s}, \frac{\tau T \cdot F_e^A}{C_0}\right\}, \quad (7b)$$

which correspond to the sensing service capacity of each ISAC device and each AP in the network, respectively.

D. Problem Formulation

Our objective is to satisfy the demands for the sensing and communication services in the upcoming reservation window with the minimal resource consumption. To achieve this objective, a decision $\Phi = \{D_{\max}^{I,U}, \rho_c, X_c^A, X_s^I, X_s^A, F_e^A\}$ is made, which consists of the radius of the on-device sensing region, i.e., $D_{\max}^{I,U}$, the active probability for uplink communication of each ISAC device, i.e., ρ_c, the amount of reserved spectrum resources, i.e., X_c^A, X_s^A, and X_s^I, and the amount of reserved edge computing resources, i.e., F_e^A. An optimization problem is formulated as follows:

$$(P1): \min_{\Phi} \quad Z = \omega\left(Z_c^A + Z_s^I + Z_s^A\right) + \xi Z_e^A \quad (8a)$$

$$\text{s.t.} \quad 0 \leq \rho_c \leq 1, \quad (8b)$$

$$X_c^A, X_s^I, X_s^A \in \mathbb{Z}_{\geq 0}, \quad (8c)$$

$$F_e^A, D_{\max}^{I,U} \in \mathbb{R}_{\geq 0}, \quad (8d)$$

$$\overline{R} \geq \hat{R}, \quad (8e)$$

$$\overline{N}_A^U + \mathbb{E}\left[N^I\right] \cdot \overline{N}_I^U \geq \mathbb{E}\left[N^U\right], \quad (8f)$$

$$\mathbb{P}\{\gamma_s \geq \widehat{\gamma}_s\} \geq \widehat{P}, \quad (8g)$$

where Z is the overall resource consumption; ω and ξ are the cost of reserving each unit of spectrum resources and edge computing resources, respectively; constraint (8e) ensures that the expected transmission rate of each ISAC device is greater than a threshold $\hat{R}$; constraint (8f) ensures that the expected number of targets that can be tracked with the requirements on the sensing data quantity and processing delay satisfied is greater than the expected number of the targets in all the RoIs in the coverage of the AP; (8g) ensures that the requirement on sensing data quality evaluated by SIR is satisfied.

Solving Problem (P1) requires the spatial modeling of ISAC devices and targets. In particular, according to (2), calculating the communication service capacity, i.e., $\overline{R}$, requires the expected number of ISAC devices in the coverage of each AP, i.e., $\mathbb{E}\left[N^I\right]$; According to (7a), the sensing capacity of each ISAC device, i.e., $\overline{N}_I^U$, depends on the spatial distributions of targets; According to (6), the sensing service demand in the coverage of each AP, i.e., $\overline{N}^U$, depends on the spatial
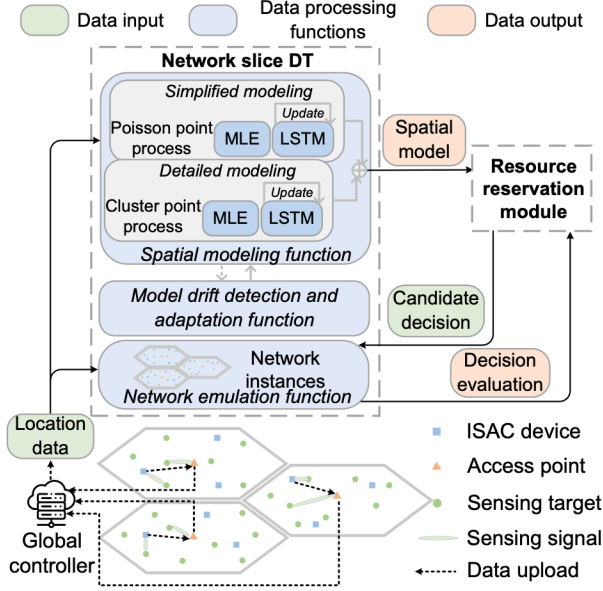
Fig. 4: The model of a slice DT.

(a) μ_k^{U} (b) σ_k^{U}

Fig. 5: Values of the parameters μ_k^{U} and σ_k^{U} in the detailed modeling across reservation windows.

distributions of the ISAC devices and the targets, respectively; Moreover, the sensing interference experienced by each ISAC device, impacting γ_{s} in (8g), is affected by the spatial distribution of the ISAC devices. However, obtaining an accurate spatial model of the ISAC devices and targets is challenging. This is because their stochastic spatial distributions can be non-stationary in an industrial CPS.

IV. NETWORK SLICE DTS FOR ADAPTIVE SPATIAL MODELING

The DT of a network slice, hereafter referred to as the *slice DT*, is a digital representation of a network slice that is established and updated by collecting and processing data from individual users and infrastructures within the network slice for the service-specific prediction and control [22]. In this section, we introduce the establishment of the slice DTs in the CPS, the model of which is illustrated in Fig. 4.

A. Location Data Collection

To establish the slice DTs, each AP collects the location data of the ISAC devices and targets, and uploads location data to the global controller every M_0 sensing frames. The location data are collected by each AP in the following way. First, the locations of the targets, that are associated with the AP for tracking in this frame, are obtained by processing the reflected sensing signals. Second, the locations of the targets associated with the ISAC devices and that of the ISAC devices are obtained and then uploaded by the ISAC devices to the AP. The location data are used as the input for the slice DTs.

B. Spatial Modeling Function

The collected location data of ISAC devices and targets are processed to derive the spatial modeling for the next reservation window, i.e., the $(k+1)$-th reservation window, for resource reservation. To cope with the potential non-stationarity of the spatial distributions across reservation windows, in
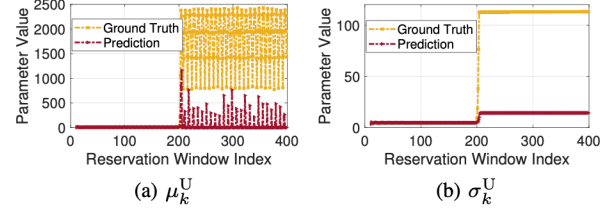
this paper, temporally non-stationary point processes [42] are exploited. Specifically, we consider the model parameters are constant in each reservation window and can change across reservation windows. To tackle the challenge in predicting the model parameters, we propose two types of spatial modeling, i.e., *detailed spatial modeling* and *simplified spatial modeling*, based on two different point processes.

1) Detailed Spatial Modeling: In the detailed spatial model, the spatial distributions of ISAC devices and targets in the k-th reservation window are jointly modeled by a Thomas cluster process. Specifically, the locations of ISAC devices are modeled by a homogeneous Poisson point process (PPP) with intensity λ_k^{I}. The relative two-dimensional locations of the targets clustering around each ISAC device follows two identical and independent normal distributions with zero mean and standard deviation σ_k^{U} [43]. In addition, the number of targets in the cluster of each ISAC device follows a Poisson distribution with mean μ_k^{U}. At the end of the k-th reservation window, using the location data collected in this reservation window, the model parameters, i.e., λ_k^{I}, σ_k^{U}, and μ_k^{U}, are determined based on the maximum likelihood estimation (MLE). For predicting the three parameters for resource reservation in the $(k+1)$-th reservation window, denoted by $\check{\lambda}_{k+1}^{\mathrm{I}}$, $\check{\sigma}_{k+1}^{\mathrm{U}}$, and $\check{\mu}_{k+1}^{\mathrm{U}}$, long short-term memory (LSTM) neural networks are established in the DT.

The detailed modeling characterizes the probability distribution of the distances between ISAC devices and targets with the model parameters μ_k^{U} and σ_k^{U}. If the parameters can be accurately predicted for the upcoming reservation window, the detailed modeling will be accurate. However, if there is a shift in the probability distribution of these parameters, referred to as *data drift*, the accuracy of parameter prediction and spatial modeling can degrade, referred to as *model drift* [21]. To illustrate this, in Fig. 5, we show the ground-truth and predicted values of the model parameters μ_k^{U} and σ_k^{U} in the detailed modeling, which are derived by MLE and the LSTM neural networks, respectively. The simulation settings are detailed in Section VI. It can be observed that after the 201-st reservation window, the ground-truth values of μ_k^{U} and σ_k^{U} exhibit a drastic increase, indicating data drift, while the predicted values show an increasing gap with the ground-truth values, indicating model drift.

2) Simplified Spatial Modeling: To cope with the model drift, a spatial modeling robust to model drift is needed. We introduce the simplified modeling, which characterizes the probability distribution of the distances between ISAC devices and targets in a simplified way. In particular, the locations of
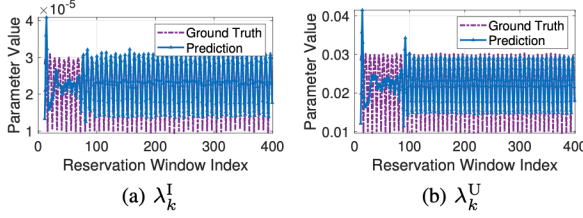
Fig. 6: Values of the parameters λ_k^{I} and λ_k^{U} in the simplified modeling across reservation windows.

the ISAC devices and targets in the k-th reservation window are modeled by two *independent* homogeneous PPPs with intensities λ_k^{I} and λ_k^{U}, respectively. Similar to the detailed modeling, using the collected data in the k-th reservation window, the intensities of the two homogeneous PPPs, i.e., λ_k^{I} and λ_k^{U}, are determined based on the MLE. The two parameters for the $(k+1)$-th reservation window, i.e., $\check{\lambda}_{k+1}^{\mathrm{I}}$, $\check{\lambda}_{k+1}^{\mathrm{U}}$, are predicted by LSTM networks based on values of the parameters in the previous K_0 windows.

In Fig. 6, with the same simulation settings as in Fig. 5, we show the ground-truth and predicted values of all the parameters in the simplified modeling, i.e., λ_k^{I} and λ_k^{U}. It can be observed that neither data drift nor model drift occurs. This observation suggests that the simplified modeling is more robust to model drift than the detailed modeling. However, it is important to note that in scenarios without model drift, the simplified modeling would yield lower accuracy than the detailed modeling.

C. Model Drift Detection and Adaptation Functions

To ensure the model accuracy, the spatial modeling function should adapt to data drift and the resulting model drift. To this end, we design a model drift detection function and a model adaptation function.

1) Model Drift Detection Function: This function monitors the prediction errors in the parameters of the spatial models and detect the model drift. By the end of the k-th time window, the errors in predicting $\{\lambda_k^{\mathrm{I}}, \lambda_k^{\mathrm{U}}, \mu_k^{\mathrm{U}}, \sigma_k^{\mathrm{U}}\}$ are evaluated by the mean absolute percentage error (MAPE) and calculated. We determine that a parameter exhibits data drift if all the MAPEs of the parameter from reservation windows $k - K_2 + 1$ to k exceed the average MAPEs from earlier reservation windows $k - K_3 + 1$ to $k - K_2$ by a threshold δ_1 or more, where $K_3 > K_2$. In addition, let H_k^{S} and $H_k^{\mathrm{D}} \in \{0, 1\}$ indicate whether the simplified modeling and the detailed modeling, respectively, experience model drift. At the end of the k-th reservation window, the following three cases are considered for model drift detection. First, if the parameter λ_k^{I}, which is shared by both modelings, exhibits data drift, we set $H_k^{\mathrm{S}} = 1$ and $H_k^{\mathrm{D}} = 1$. Second, if the parameter λ_k^{U}, which is unique to the simplified modeling, exhibits data drift, we set $H_k^{\mathrm{S}} = 1$. Third, if parameters μ_k^{U} and σ_k^{U}, which are unique to the detailed modeling, exhibit data drift, we set $H_k^{\mathrm{D}} = 1$.

2) Model Drift Adaptation Function: In this function, the following two approaches are designed to adapt to any model drift that is detected. *(i) Model Update:* When model drift is detected, LSTM neural networks for predicting the parameters

corresponding to the model drift are updated. In particular, in the reservation windows after the detection, the ground-truth values of the parameters will be collected and used to retrain the neural networks. *(ii) Model Ensemble:* When model drift is detected, the ensemble learning paradigm [44] is exploited, and an ensemble spatial model that incorporates both the simplified and detailed spatial models is output by the model drift adaptation function. In the absence of model drift, only the detailed spatial model that probably has a higher model accuracy is output.

D. Network Emulation Function

It is infeasible to directly fuse the detailed and simplified spatial models in the ensemble spatial model for resource reservation. Instead, we can evaluate and select from the two *candidate* resource reservation decisions that are respectively obtained using the two spatial models. To realize the evaluation, we introduce a network emulation function that consists of the following two steps. *1) Instance Construction:* Multiple instances of both the sensing and communication slices are created. Each instance of a communication slice involves deterministically distributed APs and ISAC devices, while each instance of a sensing slice involves deterministically distributed APs, ISAC devices, and targets. For example, the locations of all the ISAC devices and targets in the RoIs of the ISAC devices at the end of the M_0-th sensing frame in the k-th reservation window, along with the locations of the APs, are used to create one instance of the sensing slice. *2) Decision Evaluation:* A candidate resource reservation decision is implemented on each of the network instances. Then, the service demand and capacity of each network instance are measured to evaluate the corresponding candidate decision. The measurement approach and the evaluation metric for a resource reservation decision are given in Section V-B.

V. DT-BASED RESOURCE RESERVATION SCHEME

In this section, we propose a DT-based resource reservation scheme for ISAC in the CPS.

A. Spatial Modeling-Based Decision Making

In this subsection, we first derive the formulas for estimating the service demands and capacities in Problem (P1). Then, we analyze Problem (P1) for transforming the problem and deriving an efficient algorithm to obtain a candidate resource reservation decision for the $(k+1)$-th reservation window. For brevity, we omit the subscript $k+1$ in the notation of the parameters that are predicted by LSTM neural networks.

1) Estimation of the Communication Service Capacity: In both the simplified and detailed spatial models, the ISAC devices are modeled by a homogeneous PPP with the intensity $\check{\lambda}^{\mathrm{I}}$. Given that at least one ISAC device exists, the expected number of ISAC devices in the coverage of the AP with the area A_0 is given by $\mathbb{E}\left[N^{\mathrm{I}}\right] = \check{\lambda}^{\mathrm{I}} A_0 / (1 - e^{-\check{\lambda}^{\mathrm{I}} A_0})$. By substituting $\mathbb{E}\left[N^{\mathrm{I}}\right]$ in (2) with this expression, the communication service capacity $\bar{R}$ in (2) can be calculated as

$$\bar{R} = \frac{\rho_{\mathrm{c}} R_0 X_{\mathrm{c}}^{\mathrm{A}}}{1 + \left(\frac{\check{\lambda}^{\mathrm{I}} A_0}{\left(1 - e^{-\check{\lambda}^{\mathrm{I}} A_0}\right)} - 1\right) \rho_{\mathrm{c}}}. \tag{9}$$

2) Estimation of the Sensing Service Demand and Capacity: According to (6), estimating the sensing demand in the coverage of each AP, i.e., $\mathbb{E}\left[N^{\mathrm{U}}\right]$, requires (i) the probability that a target is located in the RoI of the nearest ISAC device, i.e., $\mathbb{P}\{D^{\mathrm{I,U}} \leq \hat{D}\}$, and (ii) the expected number of targets closest to the ISAC device, i.e., $\mathbb{E}\left[N_{\mathrm{I},1}^{\mathrm{U}}\right]$. First, the cumulative distribution function (CDF) of the distance between a target to the closest ISAC device, i.e., $D^{\mathrm{I,U}}$ is denoted by $\mathbb{P}\{D^{\mathrm{I,U}} \leq d^{\mathrm{I,U}}\}$ and approximated as follows. Given the simplified model, we have $\mathbb{P}\{D^{\mathrm{I,U}} \leq d^{\mathrm{I,U}}\} = 1 - \exp\left[-\left(d^{\mathrm{I,U}}\right)^2 \pi \check{\lambda}^{\mathrm{I}}\right]$, according to the contact distance distribution of a homogeneous PPP in [45]. Given the detailed model, we have $\mathbb{P}\{D^{\mathrm{I,U}} \leq d^{\mathrm{I,U}}\} = 1 - \exp\left[-(d^{\mathrm{I,U}})^2/(2(\tilde{\sigma}^{\mathrm{U}})^2)\right]$ according to the distribution of the distance in any cluster of a Thomas cluster process in [43]. Accordingly, $\mathbb{P}\{D^{\mathrm{I,U}} \leq \hat{D}\}$, can be calculated. Second, the expected number of targets closest to the ISAC device, i.e., $\mathbb{E}\left[N_{\mathrm{I},1}^{\mathrm{U}}\right]$, is approximated as follows. Given the simplified model, $\mathbb{E}\left[N_{\mathrm{I},1}^{\mathrm{U}}\right]$ is approximated as $\check{\lambda}^{\mathrm{U}}/\check{\lambda}^{\mathrm{I}}$, i.e., the ratio of the intensity of the targets to that of the ISAC devices, due to the identical randomness across different ISAC devices. Given the detailed model, $\mathbb{E}\left[N_{\mathrm{I},1}^{\mathrm{U}}\right]$ is approximated as $\check{\mu}^{\mathrm{U}}$, i.e., the expected number of targets in the cluster formed by the ISAC device.

According to (7a), estimating the sensing capacity of each ISAC device, i.e., $\overline{N}_{\mathrm{I}}^{\mathrm{U}}$, requires $\mathbb{P}\left\{D^{\mathrm{I,U}} \leq D_{\max}^{\mathrm{I,U}}\right\}$ and $\mathbb{E}\left[N_{\mathrm{I},1}^{\mathrm{U}}\right]$, which have been derived. The sensing capacity of each AP, i.e., $\overline{N}_{\mathrm{A}}^{\mathrm{U}}$ in (7b), is not affected by the spatial model.

3) Problem Analysis: We analyze the properties of Problem (P1) as follows.

Proposition 2: *In at least one optimal solution of Problem (P1), the radius of the on-device sensing region, i.e., $D_{\max}^{\mathrm{I,U}}$, is given by*

$$D_{\max}^{\mathrm{I,U}} = \left(\frac{\bar{\sigma}}{\hat{\gamma}_s} \cdot (-\ln \widehat{P}) \cdot \frac{1}{\phi_{\mathrm{I}}^2 \check{\lambda}^{\mathrm{I}}}\right)^{\frac{1}{4}} \cdot \left(\frac{X_{\mathrm{s}}^{\mathrm{I}}}{1 - \rho_{\mathrm{c}}}\right)^{\frac{1}{4}}, \quad (10)$$

which is also the maximum distance between a target and an ISAC device for satisfying the sensing SIR requirement in (8g).

Proof: Please refer to Appendix B. ∎

Based on Proposition 2, we can transform constraint (8g) equivalently into (10). To make Problem (P1) more tractable, we relax the integer decision variables, i.e., $X_{\mathrm{s}}^{\mathrm{I}}, X_{\mathrm{c}}^{\mathrm{A}}, X_{\mathrm{s}}^{\mathrm{A}}$, to real-valued variables. Then, to efficiently solve the problem, we derive necessary conditions for optimality as follows.

Proposition 3: *The optimal solution of Problem (P1) must satisfy the following three conditions:*

$$\frac{1 - \rho_{\mathrm{c}}}{\widehat{\rho_{\mathrm{s}}}} \leq \min\left\{\mathbb{E}\left[N_{\mathrm{I},1}^{\mathrm{U}}\right], \frac{\tau T \cdot F_{\mathrm{e}}^{\mathrm{I}}}{C_0}\right\}; \quad (11a)$$

$$\frac{1 - \rho_{\mathrm{c}}}{\widehat{\rho_{\mathrm{s}}}} = \mathbb{P}\left\{D^{\mathrm{I,U}} \leq D_{\max}^{\mathrm{I,U}}\right\} \cdot \mathbb{E}\left[N_{\mathrm{I},1}^{\mathrm{U}}\right]; \quad (11b)$$

$$\frac{X_{\mathrm{s}}^{\mathrm{A}}}{\widehat{\rho_s}} = \frac{\tau T \cdot F_{\mathrm{e}}^{\mathrm{A}}}{C_0}. \quad (11c)$$

Proof: Please refer to Appendix C. ∎

Condition (11a) specifies a minimum value of ρ_c since the right-hand side is independent of any decision variable in Problem (P1); (11b) gives the relation between ρ_c and $X_{\mathrm{s}}^{\mathrm{I}}$ since

$\mathbb{P}\left\{D^{\mathrm{I,U}} \leq D_{\max}^{\mathrm{I,U}}\right\}$ is a function of only these two decision variables; (11c) gives the relation between $X_{\mathrm{s}}^{\mathrm{A}}$ and $F_{\mathrm{e}}^{\mathrm{A}}$.

4) Problem Transformation and Solution: Based on Proposition 2 and Proposition 3, given the value of the decision variable ρ_{c}, the optimal values of the other four decision variables can be determined in closed forms. First, the minimum spectrum reservation for communication, $X_{\mathrm{c}}^{\mathrm{A}}$, can be obtained by converting the inequality constraint (8e) to an equality constraint. Second, the optimal amount of spectrum resources reserved for sensing by ISAC devices, $X_{\mathrm{s}}^{\mathrm{I}}$, can be found by solving (11b). Third, the optimal spectrum reservation for sensing by APs, $X_{\mathrm{s}}^{\mathrm{A}}$, can be obtained by converting the inequality constraint (8f) to an equality constraint. Given the optimal $X_{\mathrm{s}}^{\mathrm{A}}$, the optimal edge computing resource reservation, $F_{\mathrm{e}}^{\mathrm{A}}$, can be obtained based on (11c). As a result, the original multi-variable optimization problem can be transformed into a single-variable problem concerning ρ_{c}. The transformed problem can be solved by a brute-force search. Then, the real values in the decision are rounded up to integers. Given the detailed spatial model or the simplified spatial model, a candidate resource reservation decision can be respectively obtained.

B. Network Emulation-Based Decision Evaluation

Based on the network emulation function of the slice DT in Section IV-D, a candidate resource reservation decision, i.e., Φ, can be evaluated in the following way.

1) Emulating the Communication Service Provision: Evaluating the *average* transmission rate of ISAC devices requires network emulation over a long period. To reduce the complexity, we use the *expectation* of the transmission rate derived in (9). Given the location data of ISAC devices in all the constructed network instances, the intensity of ISAC devices is determined by MLE and used to replace the one predicted by an LSTM network, i.e., $\check{\lambda}^{\mathrm{I}}$ in (9). Then, given the value of ρ_c in a resource reservation decision Φ, the lower bound of the expected achievable transmission rate, i.e., $\bar{R}$, is calculated as the network emulation-based estimation of the communication service capacity. The evaluation metric chosen here is the relative difference between the service demands and capacities. Specifically, for the communication service, the relative difference is denoted by $\Delta_{\mathrm{c}}(\Phi)$ and calculated as: $\Delta_{\mathrm{c}}(\Phi) = (|\bar{R} - \hat{R}|)/\hat{R}$, which can reflect both the resource over-provision, where the communication capacity exceeds the communication demand, i.e., $\bar{R} > \hat{R}$, and resource under-provision, i.e., $\bar{R} < \hat{R}$.

2) Emulating the Sensing Service Provision: Similarly, given the candidate decision Φ, the number of the ISAC devices, the number of targets that can be monitored by the ISAC devices, and the number of targets that reside in the RoIs of all the ISAC devices in the network instances are obtained and averaged as the network emulation-based estimation of $\mathbb{E}[N^{\mathrm{I}}]$, $\overline{N}_{\mathrm{I}}^{\mathrm{U}}$, and $\overline{N}^{\mathrm{U}}$, respectively. The relative difference between the service demand and the service capacity for the sensing service is denoted by $\Delta_{\mathrm{c}}(\Phi)$ and calculated as $\Delta_{\mathrm{s}}(\Phi) = |\overline{N}^{\mathrm{U}} - \left(\overline{N}_{\mathrm{A}}^{\mathrm{U}} + \mathbb{E}\left[N^{\mathrm{I}}\right] \cdot \overline{N}_{\mathrm{I}}^{\mathrm{U}}\right)|/\overline{N}^{\mathrm{U}}$.

3) Overall Evaluation of the Resource Reservation Decision: Given a candidate resource reservation decision Φ, the

average difference between the demands and capacities for the sensing and communication services is denoted by $\Delta(\Phi)$ and calculated as $\Delta(\Phi) = (\Delta_c(\Phi) + \Delta_s(\Phi))/2$, which is used for the overall evaluation of the resource reservation decision.

C. Overall Resource Reservation Scheme

At the end of the k-th reservation window, based on the model drift detection result, the slice DTs output a spatial model for the $(k + 1)$-th reservation window. A resource reservation scheme that can adapt to the spatial model is introduced as follows.

- *Case 1 (Model Drift Not Detected):* When model drift is not detected, i.e., $H_k^S = 0$ and $H_k^D = 0$, only the detailed spatial model is output from the slice DT. The resource reservation decision based on the detailed spatial model, denoted by Φ^D, is obtained according to Section V-A, and adopted for the $(k + 1)$-th reservation window.
- *Case 2 (Model Drift Detected):* When model drift is detected for the detailed modeling, i.e., $H_k^S = 1$ or $H_k^D = 1$, the slice DT will output an ensemble spatial model consisting of both the detailed and the simplified spatial models. In this case, the two candidate resource reservation decisions are respectively derived as Φ^S and Φ^D. Then, the two candidate decisions are respectively evaluated by the network emulation function according to Section V-B, and the evaluation results $\Delta(\Phi^S)$ and $\Delta(\Phi^D)$, reflecting the respective discrepancies between service demands and service capacities, are obtained. The candidate decision with the minimal demand-capacity discrepancy is selected as the final resource reservation decision for the $(k + 1)$-th reservation window.

VI. SIMULATION RESULTS

In this section, we demonstrate by simulations the performance of the DT-based adaptive spatial modeling and resource reservation scheme.

A. Simulation Settings and Benchmarks

The locations of the ISAC devices and targets in an industrial CPS at any time instant are set as follows. The locations of ISAC devices are generated following a homogeneous PPP, while the locations of targets are generated in two steps. In the first step, the number of targets in the RoI of each ISAC device is determined by sampling from a Poisson distribution. In the second step, targets are randomly and uniformly generated within the RoI of each ISAC device. A thinning approach is then used to determine whether to retain each target based on a probability, until the predetermined number of targets for each ISAC device is reached. Specifically, two types of ISAC devices are considered, with devices set to type I and type II with probabilities ν and $1 - \nu$, respectively. The probabilities to retain a generated target for type I and type II ISAC devices are given by $D^{I,U}/\hat{d}$ and $1 - D^{I,U}/\hat{d}$, respectively, where $D^{I,U}$ is the distance between the target and the ISAC device, and $\hat{d}$ is the radius of the RoI. The other main simulation settings are given in Table I.

To generate the location data across reservation windows, the parameters of the homogeneous PPP and the Poisson distribution are changed based on the absolute values of cosine functions with the angular frequency $\pi/8$. Each simulation run includes 400 consecutive reservation windows, and for each simulation setting, we conduct 5 simulation runs and evaluate the average performances. The following three performance metrics are adopted: *1) Actual Service Satisfaction Ratio:* This metric represents the average satisfaction ratios for the sensing and communication services as observed at the end of each reservation window. Each service's satisfaction ratio is calculated as the minimum between 1 and the ratio of the service capacity to the service demand; *2) Overall Resource Consumption:* This metric represents the overall cost of reserving the spectrum resources and edge computing resources for the sensing and communication services, as defined in (8a); *3) Modeling Error:* This metric represents the average prediction error of the parameters in a spatial model. A sliding average approach is used with the width of 20 reservation windows.

TABLE I: System parameters in simulation

Parameter	Value
Beamwidth of ISAC devices for sensing, ϕ_I	$\pi/6$
Bandwidth of a communication subcarrier, $B_{c,0}$	0.015 MHz
Transmit power for sensing, P_s	20 dBm
Bandwidth of a sensing band, $B_{s,0}$	1 MHz
Average radar cross section, $\bar{\sigma}$	0.5 m^2
Side length of each AP's coverage, r_0	500 m
Duration of a time slot, τ	1 ms
Number of time slots in a sensing frame, T	1000
Number of sensing frames in a reservation window, M	500
Location data collection period in sensing frames, M_0	10
Number of APs in the cluster, L	3
CPU cycles for sensing one target, C_0	1×10^8 cycles
CPU frequency of each ISAC device, F_e^I	2 GHz
SIR requirement for sensing, $\hat{\gamma}_s$	20 dB
Threshold for SIR requirement satisfaction, $\hat{P}$	0.95
Communication throughput requirement, $\hat{R}$	1 kb/slot
Sensing frequency requirement for each target, $\hat{\rho}_s$	0.05
Radius of the RoI for each ISAC device, $\hat{D}$	10 m
Cost of reserving a unit of spectrum resources, ω	1
Cost of reserving a unit of edge computing resources, ξ	1×10^{-3}
Parameters in model drift detection, $\{K_1, K_2, K_3, \delta_1\}$	$\{5, 3, 13, 0.2\}$

We compare our proposed DT-based adaptive modeling with the following benchmarks:

- **Simplified Modeling (Ideal Case):** Use the simplified spatial modeling with perfect parameter prediction.
- **Simplified Modeling:** Use the simplified spatial modeling with LSTM neural networks to predict model parameters, while the proposed model drift detection and the model update approaches are not implemented.
- **Detailed Modeling (Ideal Case):** Use the detailed spatial modeling with perfect parameter prediction.
- **Detailed Modeling:** Use the detailed spatial modeling with LSTM neural networks to predict model parameters, while the proposed model drift detection and model update approaches are not implemented.

B. Effectiveness of DT-based Adaptive Modeling

In this subsection, we demonstrate the performance of the DT-based adaptive spatial modeling and resource reservation scheme. In each simulation, the value of ν is set to 0.1 and 0.7
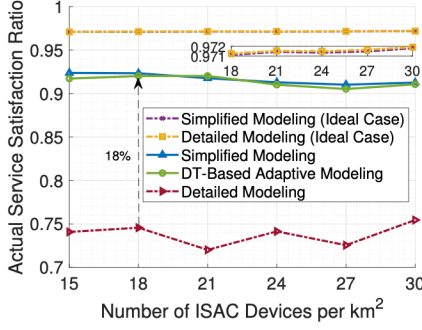
Fig. 7: Actual service satisfaction ratio versus average number of ISAC devices per square kilometre.
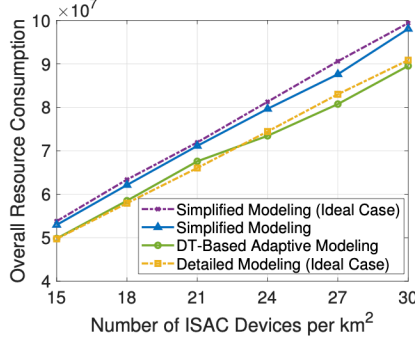

Fig. 8: Overall resource consumption versus average number of ISAC devices per square kilometre.

Fig. 9: Modeling error across reservation windows.

before and after the 201-st reservation window. The average number of targets in the RoI of each ISAC device is set to be 5.5 and that of the ISAC devices varies from 15 to 30 per square kilometre. In Fig. 7, we show the actual service satisfaction ratio, and in Fig. 8, we show the overall resource consumption.

First, in the two ideal cases where parameter predictions are perfect, we compare the performances of the detailed modeling and simplified modeling. It can be observed from Fig. 7 that the use of a single model in the ideal cases result in similarly high service satisfaction ratios. From Fig. 8, it can be observed that the use of the detailed modeling in the ideal case results in the resource reservation decisions that consume less resources than the use of simplified modeling in the ideal case. This is because, even though the simplified modeling can accurately estimate the expected number of targets in the whole RoI of each ISAC device, it underestimates that in the on-device sensing region, which is an inner circle of the RoI. Consequently, the demand for sensing services can be accurately estimated, whereas the sensing capacity of ISAC devices is under-estimated.

Second, in the non-ideal cases where model parameters are predicted by LSTM neural networks, we compare the performances of the simplified modeling, detailed modeling, and the DT-based adaptive modeling. Unlike in the ideal cases where the detailed modeling outperforms the simplified modeling, in the non-ideal cases, it can be observed from Fig. 7 that, using the detailed modeling scheme results in a much lower actual service satisfaction ratio than using the simplified modeling. This is because, as shown in Fig. 5, after the value of ν changes in the 201-st reservation window, the
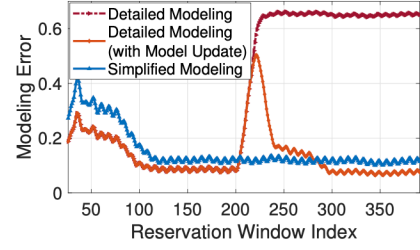
detailed modeling exhibits model drift, while the simplified modeling does not. In addition, it can be observed from Fig. 7 that using the DT-based adaptive spatial modeling results in nearly the same service satisfaction ratio as the simplified modeling. In addition, it can be observed from Fig. 8 that, the use of the DT-based adaptive spatial modeling results in lower resource consumption compared with the simplified modeling.

From the observations in the non-ideal cases, the DT-based adaptive modeling scheme achieves the best performance. In the following subsections, we illustrate the benefits of the model update and model ensemble approaches, respectively, where the average number of targets in the RoI of each ISAC device is 5.5 and that of the ISAC devices is 15.

C. Effectiveness of Model Update

In Fig. 9, we show the modeling error across reservation windows. From Fig. 9, it can be observed that, after the value of ν changes in the 201-st reservation window, the modeling error of the detailed modeling drastically increases, while that of the simplified modeling does not. In contrast, with model drift detection and model update by retraining the LSTM neural networks, the modeling error of the detailed modeling quickly falls down after the increase. This observation demonstrates that the model update approach can enable the detailed modeling to address model drift and thus become suitable for resource reservation in the presence of model drift.

D. Effectiveness of Model Ensemble

In this subsection, we demonstrate the performance with the model drift of the detailed modeling occurring at different intervals. The interval is referred to as *model drift interval* measured in the numbers of reservation windows. To simulate an occurrence of the model drift, the value of ν alters between 0.1 and 0.7.

First, in Fig. 10, we show the per-window performances from the 240-th to the 270-th reservation window, where the model drift interval is 120 reservation windows. In Fig. 10a, we show the model drift detection result. From Fig. 10a, it can be observed that the model drift, occurring in the 241-st reservation window, is successfully detected at the 244-th reservation window. In Fig. 10b, we show the actual service satisfaction ratio. From the figure, it can be observed that, after the model drift occurs, the actual service satisfaction ratio, by using the detailed modeling with the model update, first decreases, and then increases. In addition, it can be observed that by using the model ensemble

(a) Model drift indicator H_k^{D}.

(b) Actual service satisfaction ratio.

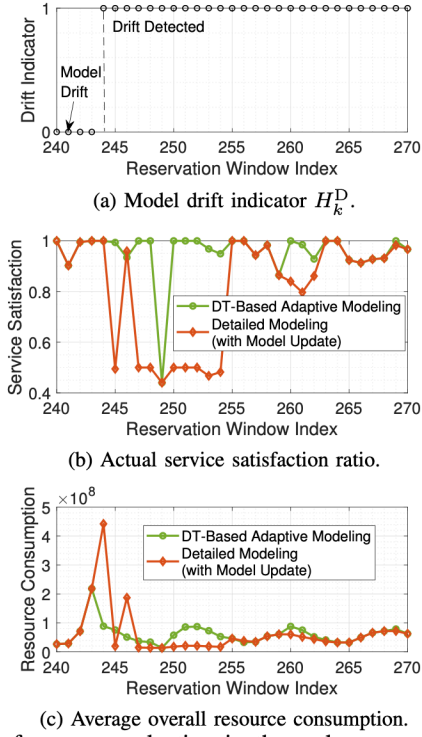(c) Average overall resource consumption.

Fig. 10: Performance evaluation in the early reservation windows after model drift occurs.
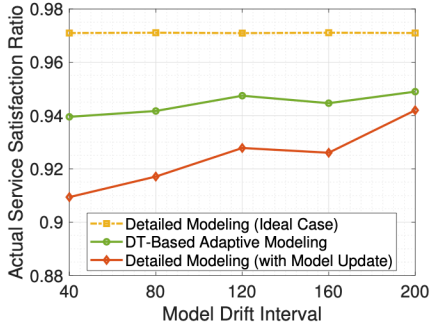

Fig. 11: Actual service satisfaction ratio versus model drift interval.

approach in the DT-based adaptive modeling, a higher service satisfaction ratio can be achieved in multiple reservation windows. This is because, by using the model ensemble approach, when model drift is detected, both the detailed and simplified spatial models are output from the slice DT for resource reservation, and the network emulation function in the slice DT evaluates the resource reservation decisions derived from the two spatial models, and selects the better decision. Similarly, from Fig. 10c, it can be observed that, the model ensemble approach demonstrates its effectiveness by preventing resource over-provision in the 244-th and 246-th reservation windows, while avoiding under-provision in the remaining windows between the 244-th and 254-th.

Second, we show the average performance across reservation windows when the model drift interval takes different values. In Fig. 11 and Fig. 12, we show the actual service satisfaction ratio and the overall resource consumption, respectively. From the two figures, it can be observed that compared with always using the detailed modeling, using the model ensemble approach in the DT-based adaptive modeling
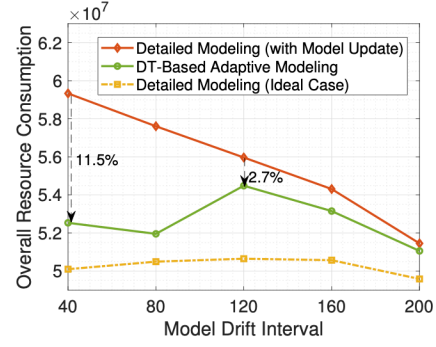

Fig. 12: Overall resource consumption versus model drift interval.

improves the actual service satisfaction ratio and decreases the overall resource consumption. In addition, it can also be observed from the two figures that, with a longer model drift interval, the advantage of DT-based adaptive modeling, in terms of improving the actual service satisfaction and reducing the resource consumption, diminishes. This is because, a longer model drift interval reduces the frequency of model drift and, consequently, the time percentage when the model ensemble approach is applied.

The observations in this subsection reveal that it is not always beneficial to use a detailed spatial modeling for resource management, especially when characterizing the detailed spatial information can experience frequent model drifts. Instead, with our proposed DT-based adaptive spatial modeling, detailed spatial information can be properly exploited for effective resource management.

VII. Conclusion

In this paper, we have proposed a DT-based proactive resource management scheme for ISAC in industrial CPSs. Our proposed DT design enables the adaptive update and ensemble of multiple point process-based spatial models for robust spatial modeling in non-stationary industrial environments. Moreover, a network emulation function has been developed in the DTs to accurately evaluate and flexibly select from resource reservation decisions given different modeling approaches. In addition to the network-level modeling, our proposed scheme can be applied to model the service demands of individual users for proactive resource management. For future work, we will investigate the establishment and update of user DTs to model individual users' differentiated and dynamic attention patterns towards various targets, enabling user-centric service provision in industrial CPSs.

Appendix A
Proof of Proposition 1

If the device is scheduled for communication in the slot, we have $R = X_{\mathrm{c}}^{\mathrm{I}} R_0$; and otherwise, $R = 0$. As a result, the expected transmission rate for the ISAC device is

$$\mathbb{E}_{N_{\mathrm{c}}^{\mathrm{I}}}[R] = \rho_{\mathrm{c}} \cdot \mathbb{E}_{N^{\mathrm{I}}}\left[\mathbb{E}_{N_{\mathrm{c}}^{\mathrm{I}}}\left[X_{\mathrm{c}}^{\mathrm{I}} R_0 | N^{\mathrm{I}}\right]\right] \tag{12a}$$

$$\geq \rho_{\mathrm{c}} \cdot \mathbb{E}_{N^{\mathrm{I}}}\left[\frac{R_0 X_{\mathrm{c}}^{\mathrm{A}}}{1 + (N^{\mathrm{I}} - 1)\rho_{\mathrm{c}}}\right] \tag{12b}$$

$$\geq \rho_{\mathrm{c}} \cdot \frac{R_0 X_{\mathrm{c}}^{\mathrm{A}}}{1 + (\mathbb{E}[N^{\mathrm{I}}] - 1)\rho_{\mathrm{c}}}, \tag{12c}$$

where (12b) holds since, based on Jensen's inequality, we have

$$\mathbb{E}_{N_c^I}\left[X_c^I | N^I\right] \geq \frac{X_c^A}{\mathbb{E}_{N_c^I}\left[N_c^I | N^I\right]} = \frac{X_c^A}{1 + (N^I - 1)\rho_c}, \quad (13)$$

and (12c) holds also due to the Jensen's inequality.

APPENDIX B
PROOF OF PROPOSITION 2

Under both the simplified modeling and the detailed modeling, the targets are modeled to be uniformly distributed in various directions around each ISAC device. As a result, the directions of the beams formed by ISAC devices in the sensing mode are independently and uniformly distributed in $[0, 2\pi)$ [9], [20]. In addition, since ISAC devices independently access each spectrum band for the sensing with the probability $(1 - \rho_c)/X_s^I$, based on the property of PPPs, the ISAC devices that access the same spectrum band for sensing form a thinned homogeneous PPP with the intensity $\check{\lambda}^I \cdot (1 - \rho_c)/X_s^I$. According to [9, Proposition 1], the CDF of the strongest interference I_s for the ISAC device is :

$$\mathbb{P}\{I_s \leq i_s\} = \exp\left(-\frac{\check{\lambda}^I \cdot (1 - \rho_c)}{X_s^I} \cdot \frac{\phi_I^2}{4\pi} \cdot \left(\frac{P_s G_m^2 c^2}{(4\pi f_s)^2}\right) \cdot i_s^{-1}\right). \quad (14)$$

Since $\gamma_s = P_e/I_s$, the probability that γ_s is higher than the threshold γ_s is

$$\mathbb{P}\{\gamma_s \geq \hat{\gamma}_s\} = \mathbb{P}\{I_s \leq \frac{P_e}{\hat{\gamma}_s}\}, \quad (15)$$

which should be greater than $\hat{P}$ to satisfy the sensing quality requirement. Therefore, we have

$$P_e \geq \hat{\gamma}_s \left(-\ln \hat{P}\right)^{-1} \cdot \left(\frac{\phi_I^2 (1 - \rho_c)\lambda_1^I}{4\pi X_s^I}\right) \cdot \frac{P_s G_m^2 c^2}{(4\pi f_s)^2}, \quad (16)$$

The power received sensing signals, i.e., P_e, is negatively correlated with the distance between the ISAC device and the target, i.e., D. As a result, to satisfy (16), there exists a maximum value of the distance. By substituting P_e in (16) with its calculation formula, the maximum distance can be calculated as the right-hand side of (10).

If there exist more than one optimal solutions for Problem (P1), consider $\Phi = \{\rho_c, X_c^U, X_s^I, X_s^A, F_e^A, D_{\max}^{I,U}\}$ as one of the optimal solutions. According to the proof in the first step, $D_{\max}^{I,U}$ should be equal to or smaller than the term on the right-hand side of (10) to make constraint (8g) in Problem (P1) satisfied. As a result, we consider the following two cases.

- Case 1: $D_{\max}^{I,U}$ is equal to the term on the right-hand side of (10). In this case, the considered optimal solution makes (10) satisfied.
- Case 2: $D_{\max}^{I,U}$ is smaller than the term on the right-hand side of (10). In this case, we can increase $D_{\max}^{I,U}$ to equal the term on the right-hand side of (10). which does not impact the overall resource consumption and ensures that all constraints in Problem (P1) remain satisfied. Accordingly, the solution after the increase of $D_{\max}^{I,U}$ is still optimal and makes (10) satisfied.

If there exists one unique optimal solution for Problem (P1), for the optimal solution, $D_{\max}^{I,U}$ must be equal to the term on the right-hand side of (10), i.e., making (10) satisfied. This is because, otherwise, according to the discussion in Case 2, we can find another optimal solution for Problem (P1).

APPENDIX C
PROOF OF PROPOSITION 3

We respectively prove the three necessary conditions in (11).

First, defined in (7a), an upper bound of the expected number of targets that can be sensed by the ISAC device is

$$\overline{N}_I^U = \min\left\{\mathbb{P}\left\{D^{I,U} \leq D_{\max}^{I,U}\right\} \cdot \mathbb{E}\left[N_{I,1}^U\right], \frac{1 - \rho_c}{\hat{\rho}_s}, \frac{\tau T \cdot F_e^I}{C_0}\right\}, \quad (17)$$

As a result, if $(1 - \rho_c)/\hat{\rho}_s$ is greater than $\mathbb{E}[N_{I,1}^U]$ or $\tau T \cdot F_e^I/C_0$, we can find a greater ρ_c which decreases the amount of required spectrum resources, i.e., X_c^A, while keeping all the other parts of Problem (P1), including $\overline{N}_I^U$, unaffected. Therefore, for the optimal solutions to Problem (P1), ρ_c should satisfy the condition in (11a):

$$\frac{1 - \rho_c}{\hat{\rho}_s} \leq \min\left\{\mathbb{E}\left[N_{I,1}^U\right], \frac{\tau T \cdot F_e^I}{C_0}\right\}. \quad (18)$$

Second, with the necessary condition, (17) reduces to

$$\overline{N}_I^U = \min\left\{\mathbb{P}\left\{D^{I,U} \leq D_{\max}^{I,U}\right\} \cdot \mathbb{E}\left[N_{I,1}^U\right], \frac{1 - \rho_c}{\hat{\rho}_s}\right\}. \quad (19)$$

According to the expression derived in Section V-A, $\mathbb{P}\left\{D^{I,U} \leq D_{\max}^{I,U}\right\}$ increases with $D_{\max}^{I,U}$ which increases with X_s^I and decreases with ρ_c, and $\mathbb{E}\left[N_{I,1}^U\right]$ is not affected by any decision variables. As a result, first, if $\mathbb{P}\left\{D^{I,U} \leq D_{\max}^{I,U}\right\} \cdot \mathbb{E}\left[N_{I,1}^U\right] > (1 - \rho_c)/\hat{\rho}_s$, we can find a smaller X_s^I while keeping all the other parts of Problem (P1) including $\overline{N}_I^U$ unaffected. Second, if $\mathbb{P}\left\{D^{I,U} \leq D_{\max}^{I,U}\right\} \cdot \mathbb{E}\left[N_{I,1}^U\right] < (1 - \rho_c)/\hat{\rho}_s$, we can find a greater ρ_c which (i) increases $\overline{N}_I^U$ such as to decrease the amount of spectrum and computing resources required for target tracking by the APs; (ii) decreases the amount of required spectrum resources, i.e., X_c^A. To conclude, for the optimal solutions to (P2), the condition in (11b) should be satisfied:

$$\frac{1 - \rho_c}{\hat{\rho}_s} = \mathbb{P}\left\{D^{I,U} \leq D_{\max}^{I,U}\right\} \cdot \mathbb{E}\left[N_{I,1}^U\right]. \quad (20)$$

Third, as for the necessary condition (11c), similarly, if it is violated, we can find a smaller amount of required spectrum resources, i.e., X_s^A, or computing resources, i.e., F_e^A without affecting all the other parts of Problem (P1).

REFERENCES

[1] S. Hu, J. Gao, X. Huang, C. Zhou, M. He, and X. Shen, "Model drift-adaptive resource reservation in ISAC networks: A digital twin-based approach," in *Proc. IEEE/CIC Int. Conf. Commun. China (ICCC)*, 2024, to be published.

[2] M. Korki, J. Jin, and Y.-C. Tian, "Real-time cyber-physical systems: State-of-the-art and future trends," in *Handbook of Real-Time Computing*. Springer, 2022, pp. 509–540.

[3] J. Jin, K. Yu, J. Kua, N. Zhang, Z. Pang, and Q.-L. Han, "Cloud-fog automation: Vision, enabling technologies, and future research directions," *IEEE Trans. Ind. Informat.*, vol. 20, no. 2, pp. 1039–1054, 2024.

[4] G. Zhu, Z. Lyu, X. Jiao, P. Liu, M. Chen, J. Xu, S. Cui, and P. Zhang, "Pushing AI to wireless network edge: An overview on integrated sensing, communication, and computation towards 6G," *Sci. China Technol. Sci.*, vol. 66, no. 3, p. 130301, 2023.

[5] Y. Cui, H. Ding, L. Zhao, and J. An, "Integrated sensing and communication: A network level perspective," *IEEE Wireless Commun.*, vol. 31, no. 1, pp. 103–109, 2024.

[6] Y. Liu, D. Lan, Z. Pang, M. Karlsson, and S. Gong, "Performance evaluation of containerization in edge-cloud computing stacks for industrial applications: A client perspective," *IEEE open J. Ind. Electron.*, vol. 2, pp. 153–168, 2021.

[7] Y. Zeng, J. Chen, J. Xu, D. Wu, X. Xu, S. Jin, X. Gao, D. Gesbert, S. Cui, and R. Zhang, "A tutorial on environment-aware communications via channel knowledge map for 6G," *IEEE Commun. Surveys Tuts.*, vol. 26, no. 3, pp. 1478–1519, 2024.

[8] X. Shen, J. Gao, W. Wu, K. Lyu, M. Li, W. Zhuang, X. Li, and J. Rao, "AI-assisted network-slicing based next-generation wireless networks," *IEEE Open J. Veh. Technol.*, vol. 1, pp. 45–66, 2020.

[9] A. Munari, L. Simić, and M. Petrova, "Stochastic geometry interference analysis of radar network performance," *IEEE Commun. Lett.*, vol. 22, no. 11, pp. 2362–2365, 2018.

[10] Y. Wang, Q. Zhang, Z. Wei, L. Kui, F. Liu, and Z. Feng, "Performance analysis of uncoordinated interference mitigation for automotive radar," *IEEE Trans. Veh. Technol.*, vol. 72, no. 4, pp. 4222–4235, 2023.

[11] W. Shi, J. Li, P. Yang, Q. Ye, W. Zhuang, X. Shen, and X. Li, "Two-level soft RAN slicing for customized services in 5G-and-beyond wireless communications," *IEEE Trans. Ind. Informat.*, vol. 18, no. 6, pp. 4169–4179, 2022.

[12] Q. Wang, Z. Pang, W. Liang, J. Zhang, K. Wang, and Y. Yang, "Spatiotemporal gradient-based physical-layer authentication enhanced by CSI-to-image transformation for industrial mobile devices," *IEEE Trans. Industr. Inform.*, vol. 20, no. 3, pp. 4236–4245, 2024.

[13] J. A. Marvel and R. Norcross, "Implementing speed and separation monitoring in collaborative robot workcells," *Robot. Comput. Integr. Manuf.*, vol. 44, pp. 144–155, 2017.

[14] H. Chauhan, A. Pakbaz, Y. Jang, and I. Jeong, "Analyzing trust dynamics in human–robot collaboration through psychophysiological responses in an immersive virtual construction environment," *J. Comput. Civ. Eng.*, vol. 38, no. 4, pp. 461–469, 2024.

[15] H. Zhang, Y. Zhang, X. Liu, C. Ren, H. Li, and C. Sun, "Time allocation approaches for a perceptive mobile network using integration of sensing and communication," *IEEE Trans. Wireless Commun.*, vol. 23, no. 2, pp. 1158–1169, 2024.

[16] A. Salem, K. Meng, C. Masouros, F. Liu, and D. Lopez-Perez, "Rethinking dense cells for integrated sensing and communications: A stochastic geometric view," *IEEE Open J. Commun. Soc.*, vol. 5, pp. 2226–2239, 2024.

[17] Z. Sun, S. Yan, N. Jiang, J. Zhou, and M. Peng, "Performance analysis of integrated sensing and communication networks with blockage effects," *arXiv preprint arXiv:2403.18621*, 2024.

[18] K. Meng, C. Masouros, G. Chen, and F. Liu, "Network-level integrated sensing and communication: Interference management and bs coordination using stochastic geometry," *arXiv preprint arXiv:2311.09052*, 2023.

[19] X. Gan, C. Huang, Z. Yang, X. Chen, J. He, Z. Zhang, C. Yuen, Y. L. Guan, and M. Debbah, "Coverage and rate analysis for integrated sensing and communication networks," *IEEE J. Sel. Areas Commun.*, pp. 1–15, 2024, to be published, doi:10.1109/JSAC.2024.3413989.

[20] M. Mei, M. Yao, Q. Yang, J. Wang, and R. R. Rao, "Stochastic network calculus analysis of spatial-temporal integrated sensing and communication networks," *IEEE Trans. Veh. Technol.*, pp. 1–5, 2024, to be published, doi:10.1109/TVT.2024.3357708.

[21] D. M. Manias, A. Chouman, and A. Shami, "Model drift in dynamic networks," *IEEE Commun. Mag.*, vol. 61, no. 10, pp. 78–84, 2023.

[22] X. Shen, J. Gao, W. Wu, M. Li, C. Zhou, and W. Zhuang, "Holistic network virtualization and pervasive network intelligence for 6G," *IEEE Commun. Surveys Tuts.*, vol. 24, no. 1, pp. 1–30, Firstquarter 2022.

[23] C. Zhou, J. Gao, M. Li, X. Shen, and W. Zhuang, "Digital twin-empowered network planning for multi-tier computing," *J. Commun. Inf. Netw.*, vol. 7, no. 3, pp. 221–238, 2022.

[24] X. Huang, W. Wu, S. Hu, M. Li, C. Zhou, and X. Shen, "Digital twin based user-centric resource management for multicast short video streaming," *IEEE J. Sel. Topics Signal Process.*, vol. 18, no. 1, pp. 50–65, 2024.

[25] J. Gong, Q. Yu, T. Li, H. Liu, J. Zhang, H. Fan, D. Jin, and Y. Li, "Scalable digital twin system for mobile networks with generative AI," in *Proc. 21st Annu. Int. Conf. Mobile Syst. Appl. Services*, 2023, pp. 610–611.

[26] S. Hu, M. Li, J. Gao, C. Zhou, and X. Shen, "Adaptive device-edge collaboration on DNN inference in AIoT: A digital twin-assisted approach," *IEEE Internet Things J.*, vol. 11, no. 7, pp. 12 893–12 908, 2024.

[27] F. Liu, Y. Cui, C. Masouros, J. Xu, T. X. Han, Y. C. Eldar, and S. Buzzi, "Integrated sensing and communications: Toward dual-functional wireless networks for 6G and beyond," *IEEE J. Sel. Areas Commun.*, vol. 40, no. 6, pp. 1728–1767, 2022.

[28] N. C. Luong, X. Lu, D. T. Hoang, D. Niyato, and D. I. Kim, "Radio resource management in joint radar and communication: A comprehensive survey," *IEEE Commun. Surveys Tuts.*, vol. 23, no. 2, pp. 780–814, 2021.

[29] Z. Xie, R. Li, Z. Jiang, J. Zhu, X. She, and P. Chen, "Optimal scheduling policy for time-division joint radar and communication systems: Cross-layer design and sensing for free," *IEEE Internet Things J.*, vol. 10, no. 23, pp. 20 746–20 760, 2023.

[30] H. Ju, Y. Long, X. Fang, Y. Fang, and R. He, "Adaptive scheduling for joint communication and radar detection: Tradeoff among throughput, delay, and detection performance," *IEEE Trans. Veh. Technol.*, vol. 71, no. 1, pp. 670–680, 2022.

[31] J. Chen, X. Wang, and Y.-C. Liang, "Impact of channel aging on dual-function radar-communication systems: Performance analysis and resource allocation," *IEEE Trans. Commun.*, vol. 71, no. 8, pp. 4972–4987, 2023.

[32] F. Dong, F. Liu, Y. Cui, W. Wang, K. Han, and Z. Wang, "Sensing as a service in 6G perceptive networks: A unified framework for ISAC resource allocation," *IEEE Trans. Wireless Commun.*, vol. 22, no. 5, pp. 3522–3536, 2023.

[33] Z. He, W. Xu, H. Shen, D. W. K. Ng, Y. C. Eldar, and X. You, "Full-duplex communication for ISAC: Joint beamforming and power optimization," *IEEE J. Sel. Areas Commun*, vol. 41, no. 9, pp. 2920–2936, 2023.

[34] Y. Hmamouche, M. Benjillali, S. Saoudi, H. Yanikomeroglu, and M. D. Renzo, "New trends in stochastic geometry for wireless networks: A tutorial and survey," *Proc. IEEE*, vol. 109, no. 7, pp. 1200–1252, 2021.

[35] M. Li, J. Gao, C. Zhou, L. Zhao, and X. Shen, "Digital twin-empowered resource allocation for on-demand collaborative sensing," *IEEE Internet Things J.*, pp. 1–17, 2024, to be published, doi:10.1109/JIOT.2024.3446801.

[36] P. Jia and X. Wang, "A new virtual network topology-based digital twin for spatial-temporal load-balanced user association in 6G hetnets," *IEEE J. Sel. Areas Commun.*, vol. 41, no. 10, pp. 3080–3094, 2023.

[37] H. Wang, Y. Wu, G. Min, and W. Miao, "A graph neural network-based digital twin for network slicing management," *IEEE Trans. Ind. Informat.*, vol. 18, no. 2, pp. 1367–1376, Feb. 2022.

[38] Y. Cui, W. Yuan, Z. Zhang, J. Mu, and X. Li, "On the physical layer of digital twin: An integrated sensing and communications perspective," *IEEE J. Sel. Areas Commun.*, vol. 41, no. 11, pp. 3474–3490, 2023.

[39] H. Chen, T. D. Todd, D. Zhao, and G. Karakostas, "Digital twin model selection for feature accuracy," *IEEE Internet Things J.*, vol. 11, no. 7, pp. 11 415–11 426, 2024.

[40] W. Yi, Y. Yuan, R. Hoseinnezhad, and L. Kong, "Resource scheduling for distributed multi-target tracking in netted colocated MIMO radar systems," *IEEE Trans. Signal Process.*, vol. 68, pp. 1602–1617, 2020.

[41] G. Ghatak, R. Koirala, A. De Domenico, B. Denis, D. Dardari, B. Uguen, and M. Coupechoux, "Beamwidth optimization and resource partitioning scheme for localization assisted mm-wave communication," *IEEE Trans. Commun.*, vol. 69, no. 2, pp. 1358–1374, 2021.

[42] J. A. González, F. J. Rodríguez-Cortés, O. Cronie, and J. Mateu, "Spatio-temporal point process statistics: a review," *Spatial Statist.*, vol. 18, pp. 505–544, 2016.

[43] P. D. Mankar, G. Das, and S. S. Pathak, "Modeling and coverage analysis of BS-centric clustered users in a random wireless network," *IEEE Wireless Commun. Lett.*, vol. 5, no. 2, pp. 208–211, 2016.

[44] X. Dong, Z. Yu, W. Cao, Y. Shi, and Q. Ma, "A survey on ensemble learning," *Front. Comput. Sci.*, vol. 14, pp. 241–258, 2020.

[45] X. Lu, M. Salehi, M. Haenggi, E. Hossain, and H. Jiang, "Stochastic geometry analysis of spatial-temporal performance in wireless networks: A tutorial," *IEEE Commun. Surveys Tuts.*, vol. 23, no. 4, pp. 2753–2801, 2021.